Pramana – J. Phys. (2018) 90:4
https://doi.org/10.1007/s12043-017-1498-5

N_2 adsorption on the inside and outside the single-walled carbon nanotubes by density functional theory study

FAHIMEH SHOJAIE

Department of Photonics, Institute of Science and High Technology and Environmental Sciences, Graduate University of Advanced Technology, P.O. Box 76315-117, Kerman, Iran
E-mail: f.shojaie@kgut.ac.ir

MS received 6 October 2016; revised 21 July 2017; accepted 1 August 2017; published online 11 December 2017

Abstract. The adsorption energies, bond order, atomic charge, optical properties, and electrostatic potential of nitrogen molecules of armchair single-walled carbon nanotubes (SWCNTs) and nitrogen-doped single-walled carbon nanotubes (N-SWCNTs) were investigated using density functional theory (DFT). Our results show that adsorption of the N_2 molecules on the external wall of a nanotube is more effective than on the internal wall in SWCNTs. The results show that N_2 molecule(s) are weakly bonded to SWCNTs and N-SWCNTs through van der Waals-type interactions. The interaction of N_2 molecules with SWCNTs and N-SWCNTs is physisorption as the adsorption energy and charge transfer are small, and adsorption distance is large. The electronic transitions from the highest occupied molecular orbital (HOMO) to the lowest unoccupied molecular orbital (LUMO) (H $\rightarrow$ L) have the maximum wavelength and the lowest oscillator strength. The potential sensor on the surface of pristine SWCNTs and N-SWCNTs for the adsorption of N_2 molecule(s) is investigated. The N-loaded single-walled carbon nanotube is introduced as a better N_2 molecule(s) detector when compared with SWCNTs.

Keywords. Single-walled carbon nanotubes; nitrogen-doped single-walled carbon nanotubes; adsorption energy; density functional theory; N_2 adsorption; density of states.

PACS Nos 82; 31.15.A–; 31

1. Introduction

The SWCNTs with their interesting properties have opened up several fields in nanotechnology since their discovery [1–5]. The SWCNTs have the ability to deliver bioactive molecules across cell membranes and even into the cell nuclei because of their very high specific surface areas [6,7]. The unique properties of SWCNTs have made them useful in different types of applications [8–10], for example, their excellent role as gas absorbers [11–13]. The adsorption of gases on CNTs has been intensively studied [14]. Many much gases can be detected by nanotubes. It is noteworthy that the electrical conductivity changes of the CNTs sensors are observed after adsorption of gas molecules [15]. Several experimental studies have been carried out on adsorption of N_2 gas by carbon nanotubes [16,17]. Yang *et al* observed a multistage nitrogen adsorption process in the aggregated multiwalled carbon nanotubes [18]. Zhu *et al* used non-local DFT to simulate nitrogen adsorption behaviour in SWCNT at 77 K, with diameters ranging from 0.696 to 3.001 nm [19]. Also, the adsorption of nitrogen at 77 K on square arrays of open and closed SWCNTs is simulated with the method of grand canonical ensemble Monte Carlo [16]. The isothermic adsorption of nitrogen on close-ended SWCNT bundles are measured at temperatures ranging from 81 to 94 K [14]. The adsorption isosteric heat of nitrogen molecules on the open-ended nanotube bundles was measured at temperatures ranging from 117 to 130 K [20]. A sub-nm thin SWCNT can indeed template a locked linear arrangement of N_2 molecules [21]. Experimental and Monte Carlo molecular simulation techniques were employed to investigate the adsorption phenomenon of various gases (such as nitrogen gas) on SWCNTs [22]. There are several theoretical reports of N_2 adsorption studies on (5,5) SWCNT. First-principle calculations are used on the adsorption properties of nitrogen molecule on the pentagon at the tip of a capped (5,5) SWCNTs by Ganji [23]. He showed that the adsorption of this molecule

on capped nanotube carbon is more stable, where the molecular axis is parallel to the pentagon of the substrate. Zhao *et al* studied the adsorption of N_2 gas and a variety of gas molecules on (5,5) SWCNTs and bundles based on DFT [24]. They used a one-dimensional periodic boundary condition along the tube axis and found that the interaction between the SWCNTs and gas molecules is weak and does not have a significant influence on the electronic structures of carbon nanotube. In this work, a theoretical study on the structural properties and reactivity of adsorption of nitrogen molecules on the inside and outside walls of the armchair (5,5) SWCNTs and N-SWCNTs is presented. The changes in electronic and structural properties of SWNTs and N-SWCNTs before and after the adsorption of N_2 are studied. The potential sensor on the surface of pristine SWCNTs and N-SWCNTs for the adsorption of N_2 molecule(s) is investigated.

2. Computational methods

All calculations of SWCNT properties were performed by using DMol^3 code [25] which is based on DFT. The DFT with double numerical basis set with polarization functions (DNP) was used by this code. This basis set is comparable with the Gaussian 6-31G(d,p). The main calculations presented in this work are based on the generalized gradient approximation (GGA) correction methods developed by Perdew and Wang (PW91) [26]. To depict core states, all electrons were taken into account [27]. Total energy convergence criteria for the self-consistent field (SCF) were set to 10^{-6} eV. To improve computational performance in terms of fast SCF convergence, a smearing of 0.005 Hartree was considered. All structures were considered to be minima based on the absence of imaginary frequencies, which provides a true minimum on the potential surface. Simulation studies were conducted on the C(5,5) pristine carbon nanotubes, which were used in the adsorption process of nitrogen molecules on their walls. These nanotubes contain 80 carbon atoms and 20 hydrogen atoms ($C_{80}H_{20}$). In order to decrease the boundary effects, 100 nanotube atoms were considered. The C(5,5) carbon nanotube is the most reactive nanotube [28]. The basis set superposition errors (BSSE) of the DNP basis set have been used for the counterpoise correction of the values of interaction energy [29]. The bond length between two carbons in SWCNT is 1.42 Å, which corresponds to the bond length between two carbons in sp^2 hybridization, the diameter of the nanotube is 6.78 Å, and the length of the nanotube is 9.84 Å. In order to study the effects of quantum chemical parameters on the C(5,5) carbon nanotubes, we have considered thirteen stable models with optimized configurations as shown in figure 1. The type-I SWCNT models show the adsorption of a single nitrogen molecule and the type-II SWCNT models indicate adsorption of two nitrogen molecules on the inside and outside walls of the SWCNTs. In addition, to study the effects of the presence of nitrogen impurity (N-SWNTs), seven stable configuration models have been considered which are presented in figure 2. In this work, I2 and I4 models in types I and II1, II2, II3, II8 and II9 models in type-II were doped by replacing one carbon atom by a nitrogen atom. Our results show that adsorption of N_2 molecules on the external wall of a SWCNT is more effective than on the internal wall in SWCNT.

3. Results and discussions

The quantum chemical parameters give information on the chemical reactivity of molecules. Table 1 shows the HOMOs and LUMOs for SWCNT and I1-II9 models, calculated by PW91 method. The energy levels of the HOMOs are in the range -4.235 to -4.253 eV and the energy levels of LUMOs are in the range -3.323 to -3.351 eV. A higher E_{HOMO} suggests a lower capability of accepting electrons. The lower the value of E_{LUMO} is, the more probable that the molecule would accept electrons. The type-II SWCNT models have low E_{HOMO} in comparison to type-I models. Among the type-I SWNT models, the I3 model has the highest value of E_{HOMO} and I2 model has the lowest value of E_{LUMO}. The gap between the HOMO and the LUMO energy levels is an important function of reactivity of a molecule. Figure 3 indicates that the I3 model has a low energy gap. Thus, moving an electron from the HOMO of the I3 model to its LUMO is easier than in other three I models. The energy gap (ΔE) and global hardness ($\eta = (I - A)/2$, $I = -E_{\mathrm{HOMO}}$) [30,31] of all the type-I and -II models are smaller than the pristine C(5,5) carbon nanotubes. This indicates that the reactivity of the types I and II systems are higher than that of the pristine C(5,5) carbon nanotubes. The energy gap and global hardness of $C_{79}NH_{20}$ (N-SWCNT) and N-doped models are smaller than their pristine models (see figures 3 and 4). This indicates that the reactivity of the doped systems is higher than the reactivity of their pristine systems. A small energy gap leads to a large electric conductivity at a given temperature. Thus, electric conductivity of $C_{80}H_{20}$ and models of I2, I4, II1, II2, II3, II8 and II9 increase with nitrogen doping.

The polarity of a molecule describes its dipole moment. Figure 3 shows that the type-II9 SWCNT model has the highest value of dipole moment in the gaseous phase among all the models. Figures 4 and 5

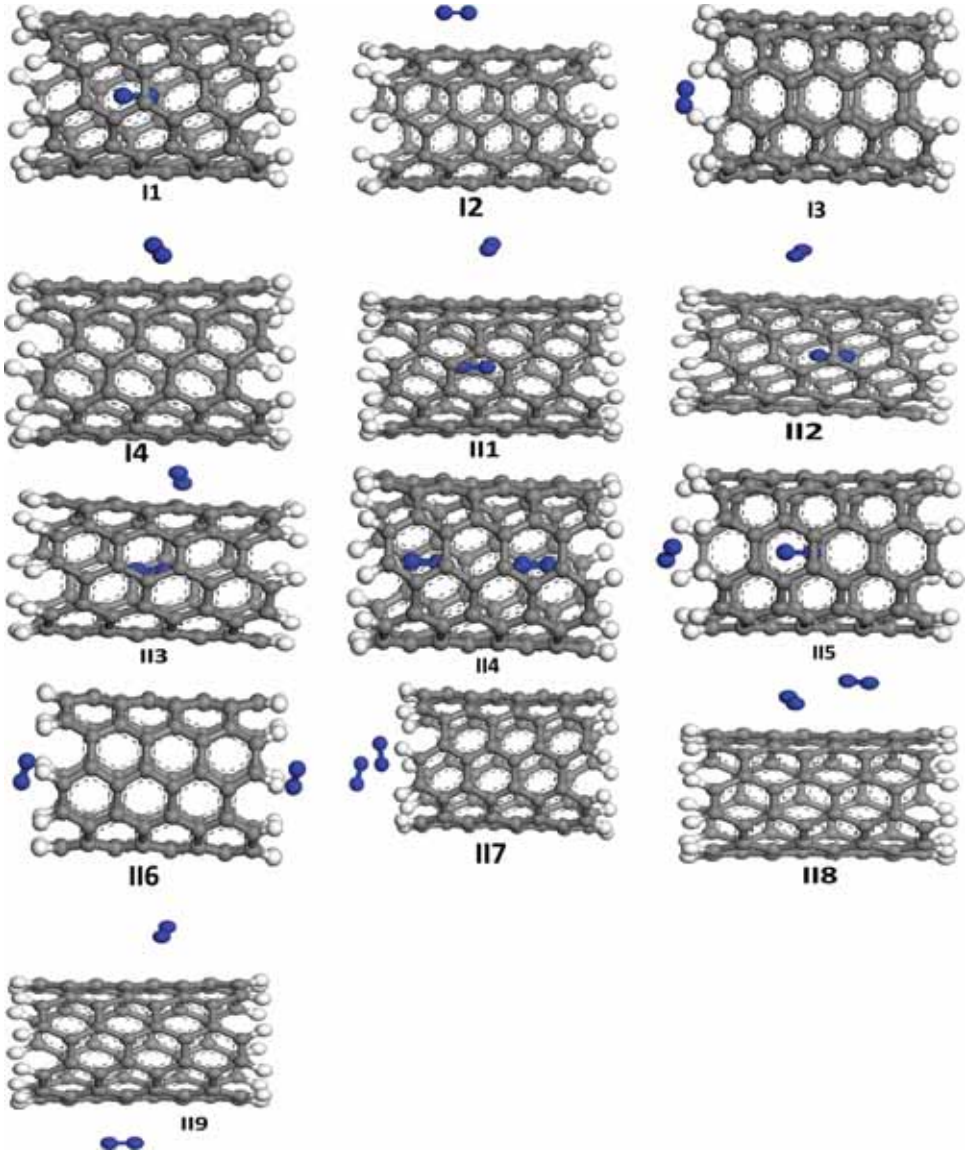

Figure 1. The optimized structures of N_2 adsorption by pristine carbon nanotubes.

show that calculated values of dipole moments for N-SWCNT, I2-N, I4-N, II1-N, II2-N, II3-N, II8-N and II9-N are higher than SWCNT, I2, I4, II1, II2, II3, II8 and II9. Adsorption of nitrogen molecule on the inside and outside walls of the pristine C(5,5) carbon nanotubes causes electron affinity ($A = -E_{\mathrm{LUMO}}$) [30], electronegativity ($\chi = (I + A)/2$) [30] and electrophilicity index ($\omega = \chi 2/2\eta$) [32] of the SWCNT complex systems to increase (see figure 3 and table 1). The ability of a SWCNT to accept electrons increases as the degree of adsorption of nitrogen molecule rises. Also, the electrophilicity index for N-SWCNT (21.034 eV) is higher than that of SWCNT. The calculated values of the electrophilicity index for I2-N, I4-N, II1-N, II2-N, II3-N, II8-N and II9-N are 80.725, 92.886, 82.090, 81.856, 81.731, 80.867 and 81.8760.084 eV, respectively. These values are the highest when compared with electrophilicity index values of I2, I4, II1, II2, II3, II8 and II9.

In order to characterise the N_2 bonds in SWCNT models and N-SWCNT, the bond length and Mayer bond order (MBO) were calculated (see tables 2 and 3). The results show that the bond order of N_2 in N_2 molecule is more than in the complexes. A higher bond order leads to a shorter bond length and a shorter bond length is associated with a stronger bond strength. The results show that there are very small differences between bond order values of N-doped models and their pristine models.

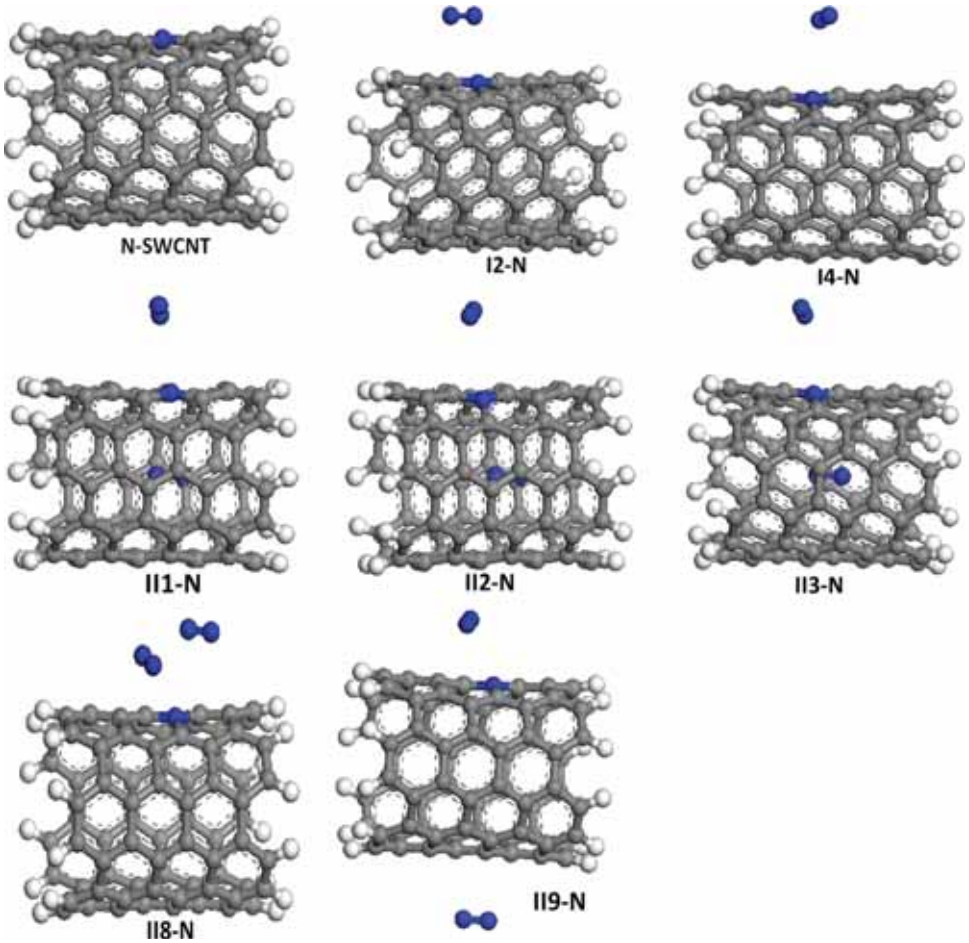

Figure 2. The optimized structures of N_2 adsorption by nitrogen-doped carbon nanotubes.

Table 1. HOMO, LUMO, electronegativity and electrophilicity indices for SWNT, I and II models.

Compounds	HOMO (eV)	LUMO (eV)	X (eV)	ω (eV)
SWNT	−4.243	−3.323	3.783	15.564
I1	−4.247	−3.329	3.788	15.643
I2	−4.253	−3.334	3.793	15.649
I3	−4.244	−3.332	3.788	15.745
I4	−4.249	−3.330	3.789	15.612
II1	−4.242	−3.347	3.795	16.091
II2	−4.246	−3.349	3.797	16.061
II3	−4.243	−3.349	3.796	16.115
II4	−4.249	−3.351	3.800	16.073
II5	−4.248	−3.339	3.793	15.816
II6	−4.235	−3.350	3.793	16.258
II7	−4.238	−3.342	3.790	16.035
II8	−4.249	−3.349	3.799	16.033
II9	−4.248	−3.348	3.798	16.032

Figures 5 and 6 show that adsorption of second N_2 molecules causes a decrease in adsorption energy and also complex SWCNT and N-SWCNT systems have negative adsorption energies which indicate thermodynamic stability. The results of our study indicate that adsorption of the N_2 molecule on the outside wall of

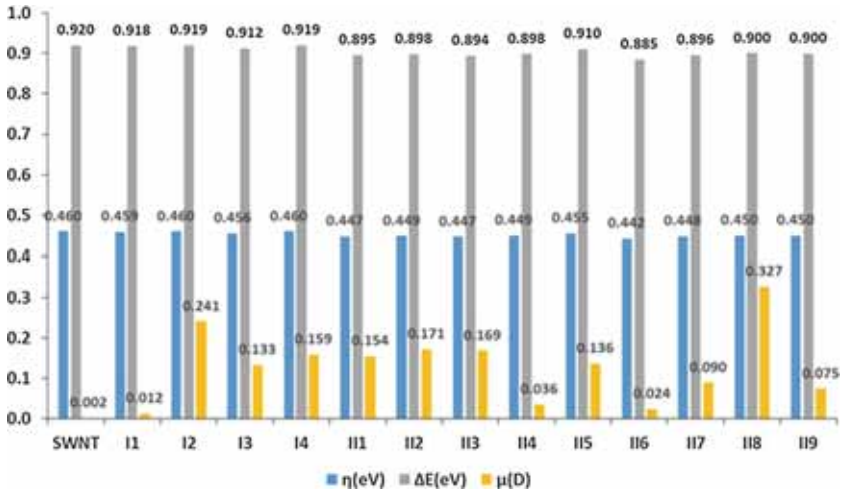

Figure 3. Diagram of energy gap, global hardness and dipole moment for SWCNT, I and II models.

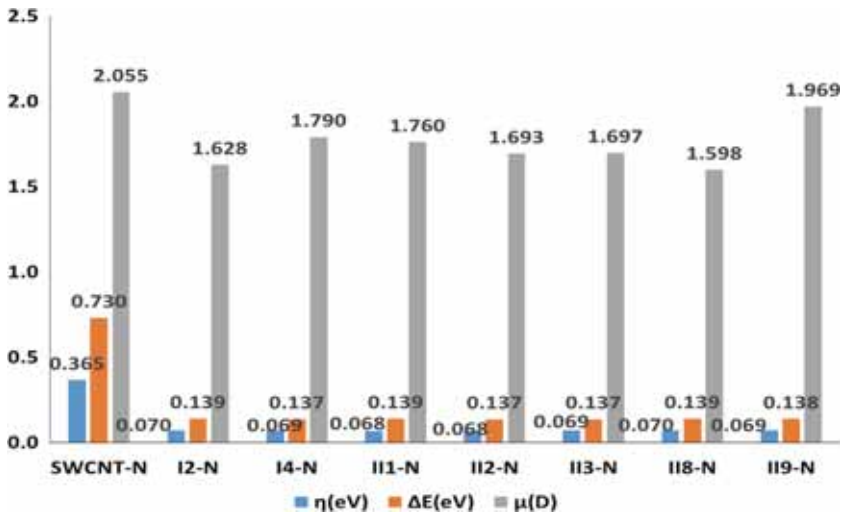

Figure 4. Diagram of energy gap, global hardness and dipole moment for N-SWCNT, N-doped models.

a SWCNT is more (see figure 5) effective than on its inside wall. The adsorption energy of the SWCNT II6 model is the lowest among all the models of SWCNT. This means the II6 model has the highest thermodynamic stability. It is seen that the adsorption energies of the N-doped models are more negative than that of the pristine models. Therefore, nitrogen impurity atom increases the adsorption of N_2 gas on the nanotube and the N-doped models are more favourable than pristine models. All SWCNT and N-SWCNT models physically adsorb N_2 molecules.

In addition, in the complexes, the distances of the N atom in the N_2 molecule and the C atom in the SWCNT are in the range 3.491–3.971 Å in pristine models and the distances of the N atom in the N_2 molecule and the N atom in the N-SWCNT are in the range 3.198–4.207 Å in N-doped models. The distance of N and N in the N_2 molecule is close to its bond length in the complexes. These results show that optimised structures of the SWCNT and N-SWCNT complex systems are in the physisorbed state.

Tables 4 and 5 show the equilibrium distances (D) and charge transfers (Q_T) of the type-I and type-2 models. The small adsorption energy (figures 5 and 6), large adsorption distance and small charge transfer indicate that N_2 molecule(s) is weakly bounded to SWCNT and N-SWCNT through van der Waals-type interactions. Therefore, these interactions can be identified as physisorption.

The charges which were calculated by Mulliken and Hirshfeld methods for N_2 molecule(s) (after adsorption), are listed in tables 6 and 7. These analyses indicated that charges have been transferred from SWCNT and N-SWCNT to N_2 molecule(s) and the charges on carbon nanotube and nitrogen-doped carbon nanotube after adsorption of N_2 molecule(s) decreased.

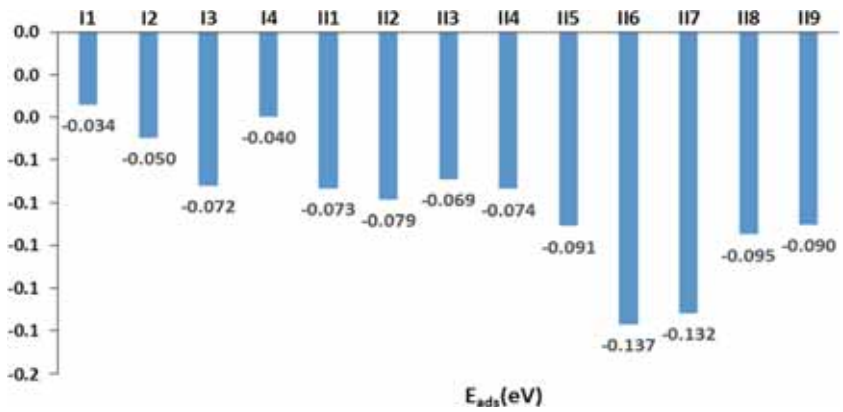

Figure 5. Diagram of N_2 adsorption energy on the SWCNT for I and II models.

Table 2. Mayer bond order (MBO) and bond distance (Å) for N_2 in N_2 molecule, I and II models.

Models	MBO	Bond length
N_2	2.979	1.107
I1	2.940	1.108
I2	2.963	1.108
I3	2.961	1.107
I4	3.000	1.107
II1	2.966	1.107
	2.940	1.108
II2	2.966	1.107
	2.940	1.108
II3	2.966	1.107
	2.941	1.108
II4	2.942	1.108
	2.942	1.108
II5	2.961	1.107
	2.940	1.108
II6	2.961	1.107
	2.961	1.107
II7	2.952	1.107
	2.957	1.107
II8	2.962	1.108
	2.964	1.107
II9	2.966	1.107
	2.964	1.107

Table 3. Mayer bond order (MBO) and bond distance (Å) for N_2 in N-doped models.

Models	MBO	Bond length
I2-N	2.978	1.107
I4-N	2.964	1.107
II1-N	2.979	1.107
	2.949	1.108
II2-N	2.981	1.107
	2.950	1.108
II3-N	2.979	1.107
	2.951	1.108
II8-N	2.978	1.107
	2.978	1.107
II9-N	2.981	1.107
	2.979	1.107

The enthalpy and the Gibbs free energy of interaction between the N_2 molecule and the SWCNT can be obtained as follows:

$$\Delta X_{\text{int}} = X_{\text{SWNT}-n\text{N}_2} - \left(X_{\text{SWNT}} + nX_{\text{N}_2}\right),$$

where X is the enthalpy (H) or the Gibbs free energy (G) and n is 1 or 2. The interaction energies of SWNT-1-N_2 (type-I models) and SWNT-2-N_2 (type-II models) in their gaseous phase and at temperature 298.15 K are listed in table 8. This table shows that adsorption of N_2 decreases the Gibbs free energy. Negative Gibbs free energies of SWCNT complex systems suggest that these interactions are spontaneous and the negative enthalpies indicate that these interactions are exothermic. If a compound has a small G, then it will have a better thermal stability. The thermal stability of type-II models is better than that of type-I models. Therefore, adsorption of N_2 increases the thermal stability.

DOS spectra of the pristine C(5,5) carbon nanotubes, type-I and type-II of SWCNT and N-SWCNT models are shown in figure 7. These spectra may help to gain a deeper understanding of the effect of N_2 adsorption on the electronic properties of the pristine C(5, 5) carbon nanotubes, SWCNT and N-SWCNT models. The DOS spectra show that adsorption of N_2 molecule(s) on the SWCNT are metallic type (band gap between the valance band and conduction band is not zero) and type-I and II of SWCNT complex systems have an energy gap close to the pristine C(5, 5) carbon nanotubes (see figure 7). The number of peaks of all DOS spectra are

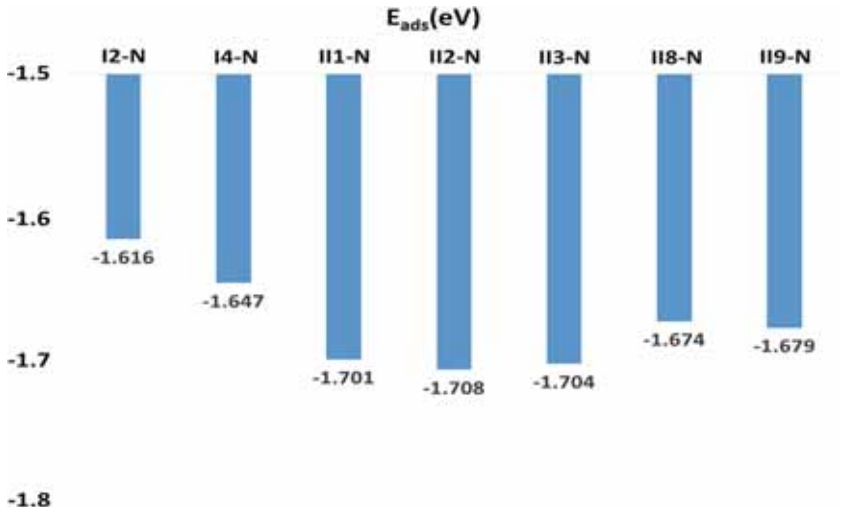

Figure 6. Diagram of N_2 adsorption energy on the N-SWCNT for N-doped models.

Table 4. The equilibrium distances and charge transfers for I and II models.

Models	D (Å) N_2–C		Q_T(e)	
			Mulliken	Hirshfeld
I1	3.889		−0.017	0.013
I2	3.393		−0.012	0.012
I3	3.614		−0.011	0.010
I4	3.564		−0.007	0.008
Models	D (Å) N_2–C	D (Å) N_2–C	Q_T(e)	
II1	3.228	3.805	−0.013	0.013
II2	3.549	3.923	−0.016	0.012
II3	3.512	3.944	−0.013	0.005
II4	3.554	2.848	−0.019	0.006
II5	3.432	3.971	−0.006	0.010
II6	3.568	3.579	−0.002	0.010
II7	3.568	3.646	−0.007	0.011
II8	3.461	3.682	−0.012	0.010
II9	3.431	3.633	−0.015	0.010

Table 5. The equilibrium distances and charge transfers for N-doped models.

Models	D (Å) N_2–N		Q_T(e)	
			Mulliken	Hirshfeld
I2-N	3.356		0.002	0.010
I4-N	3.480		0.002	−0.001
Models	D (Å) N_2–N	D (Å) N_2–N	Q_T(e)	
II1-N	3.198	3.473	0.010	0.012
II2-N	3.507	3.516	0.007	0.012
II3-N	3.505	3.451	0.003	0.011
II8-N	3.650	4.207	0.001	0.008
II9-N	3.905	10.011	0.007	0.014

Table 6. The calculated charges of N_2 molecule(s) after adsorption by Mulliken and Hirshfeld for the studied compounds.

Models	N_2 (after adsorption)	
	Mulliken	Hirshfeld
I1	− 0.001	− 0.002
I2	− 0.007	− 0.014
I3	− 0.008	0.010
I4	− 0.002	− 0.009
Models	$2N_2$ (after adsorption)	
	Mulliken	Hirshfeld
II1	− 0.004	− 0.010
II2	− 0.005	− 0.011
II3	− 0.003	− 0.010
II4	− 0.003	− 0.005
II5	− 0.009	0.009
II6	− 0.016	0.02
II7	0.001	0.045
II8	− 0.006	− 0.019
II9	− 0.008	− 0.021

Table 7. The calculated charges of N_2 molecule(s) after adsorption by Mulliken and Hirshfeld for N-doped models.

Models	N_2 (after adsorption)	
	Mulliken	Hirshfeld
I2-N	− 0.010	− 0.014
I4-N	− 0.001	− 0.007
Models	$2N_2$ (after adsorption)	
	Mulliken	Hirshfeld
II1-N	− 0.024	− 0.032
II2-N	− 0.025	− 0.033
II3-N	− 0.025	− 0.031
II8-N	− 0.009	− 0.018
II9-N	− 0.013	− 0.022

constant irrespective of N_2 adsorption, but the variation of peak heights of type-II models is more than the type-I models and the peak heights of type-I models vary more than the peak heights of pristine C(5,5) carbon nanotubes. The energy gaps of the type-I SWCNTs in the 0.001–0.008 eV range and the type-II SWNTs in the 0.010–0.056 eV range are lower than the energy gaps of the pristine C(5,5) carbon nanotubes in the same ranges. Therefore, no changes occur in the DOS of the conduction and valence bands in interaction between N_2 molecule(s) and SWCNT. The DOSs plot of interaction between N_2 molecule(s) and N-SWCNT were calculated and compared with their pristine models (see

Table 8. The enthalpy and the Gibbs free energy for I and II models.

Models		ΔH_{int} (kcal/mol)	ΔG_{int} (kcal/mol)
I	I1	− 0.961	− 9.122
	I2	− 1.032	− 7.213
	I3	− 1.204	− 9.22
	I4	− 0.482	− 8.924
II	II1	− 0.003	− 18.582
	II2	− 0.61	− 18.486
	II3	− 0.04	− 20.163
	II4	− 0.99	− 19.882
	II5	− 2.125	− 18.262
	II6	− 2.032	− 18.108
	II7	− 0.795	− 17.752
	II8	− 0.723	− 18.577
	II9	− 1.21	− 15.522

figure 7). As shown in figure 7, the DOS plots of N-doped forms were moved to the left side of the DOS plots of the pristine forms. This trend is similar to the energy gap. The energy gaps were decreased from about 0.91 eV in SWCNT models to 0.13 eV in N-SWCNT models. The energy gap of the N-SWCNT is 0.189 eV lower than the energy gap of the pristine C(5,5) carbon nanotubes. Therefore, N-SWCNT may be chosen as an appropriate candidate for the adsorption and the detection of the N_2 gas molecule(s) when compared with SWCNT.

The Perdew and Wang [26] results show that the Fermi energy is located between HOMO and LUMO energies of type-II SWCNT models (except II6). Also, figure 8 shows that Fermi energies of the pristine C(5,5) carbon nanotubes, all type-I SWCNT models and type-II6 model are the same as their HOMOs. Therefore, the pristine C(5,5) carbon nanotubes have metallic behaviour. Figure 9 shows that Fermi energies of N-doped models (I2-N, I4-N, II1-N, II2-N, II3-N, II8-N and II9-N) are the same as that of their LUMOs. Also, our calculations show that Fermi energy of the doped SWNT (5, 5) is equal to its HOMO energy.

Figure 10 shows the density of states of spin-up and spin-down electrons in type-I and type-II SWCNT and N-SWCNT models. The DOSs of spin-up and spin-down electrons are equal for all electron energies. This means that all structures of type-I and type-II SWCNT and N-SWCNT models are antiferromagnetic. Thus, the adsorption of N_2 has no effect on the magnetic properties of SWCNT and N-SWCNT.

The transitions between electronic states may be approximately interpreted in terms of one-electron transitions. The quantum calculations on electronic absorption spectra were performed. Figure 11 shows oscillator strength values which were calculated by TD-DFT.

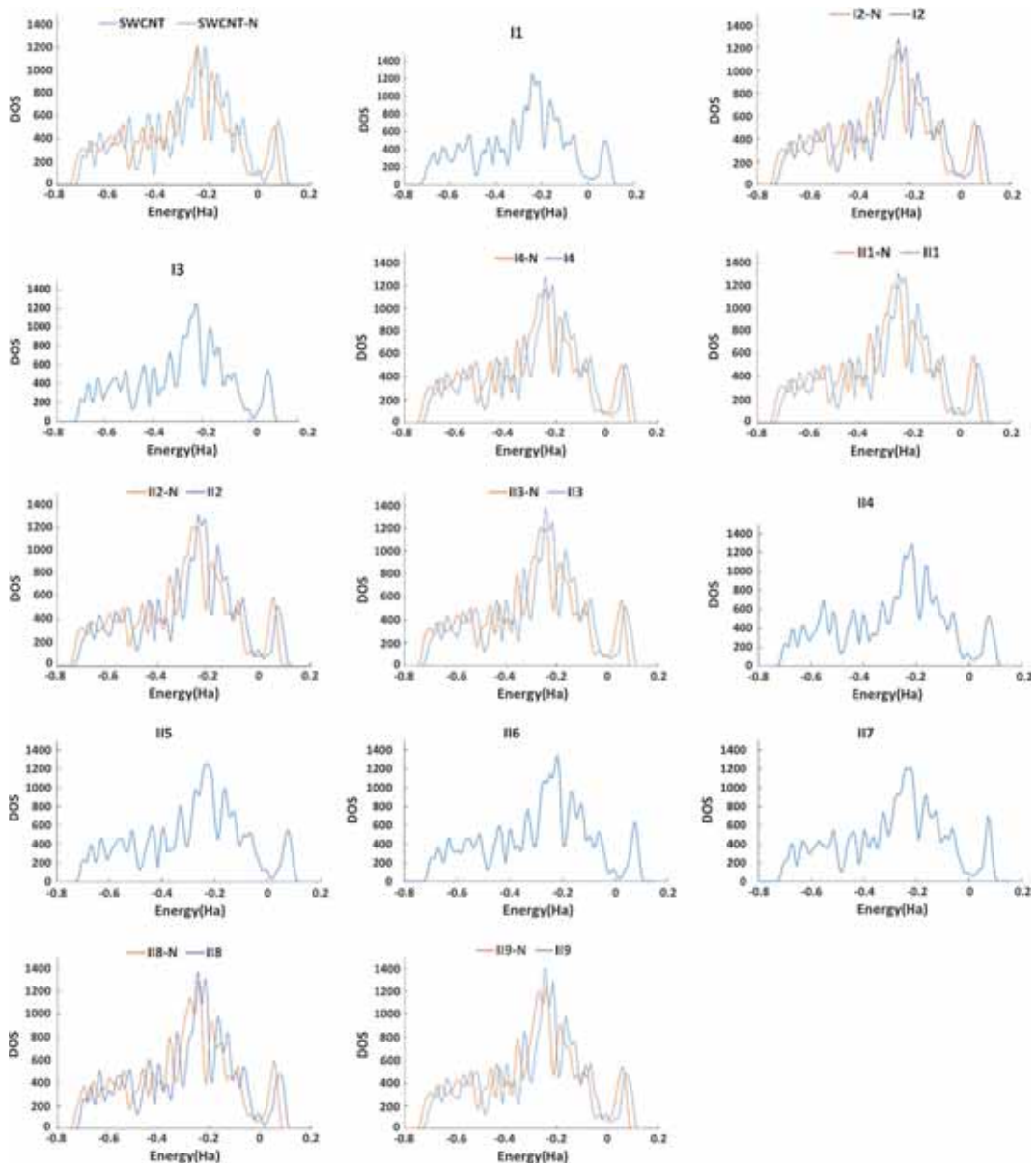

Figure 7. The spectrum of the total density of states (DOS) for N-SWCNT and N-doped models.

Tables 9 and 10 show oscillator strength and wavelength of electronic transitions of band gap (H → L) and also electronic transitions that have maximal oscillator strength. The electronic transitions from the HOMO to the LOMO (H → L) have the maximal wavelength and the lowest oscillator strength (see tables 9 and 10). The results show that the minimum wavelength of SWCNT and N-SWCNT are in the 544 and 632 nm regions, corresponding to 2.28 and 1.96 eV, respectively. These absorptions correspond to transition from the HOMO (H) to the six orbitals above the LOMO (L + 6) in SWCNT and from the first orbital below the HOMO (H − 1) to the two orbital above the LOMO (L + 2) in N-SWCNT. The most intense peaks are located between the first orbital below the HOMO and the LOMO in I1, I2, I3, I4, II1, II2, II3, II5, II6, II8, II9, I2-N, II2-N and II8-N models. The maximal wavelength of transition of H → L in II4 model is higher than other models and SWCNT. This model has a minimum wavelength in the 708 nm region, corresponding to the transition of H − 1 → L + 1 (see table 9). The maximal wavelength of transition of H → L in II8-N is higher than other models and N-SWCNT. This model has a minimum wavelength in the 586 nm region, corresponding to the transition of H → L + 6 (see table 10). The results show that the wavelength of the electronic transitions of H → L increased with adsorption of N_2 molecule(s) on the SWCNT and N-SWCNT.

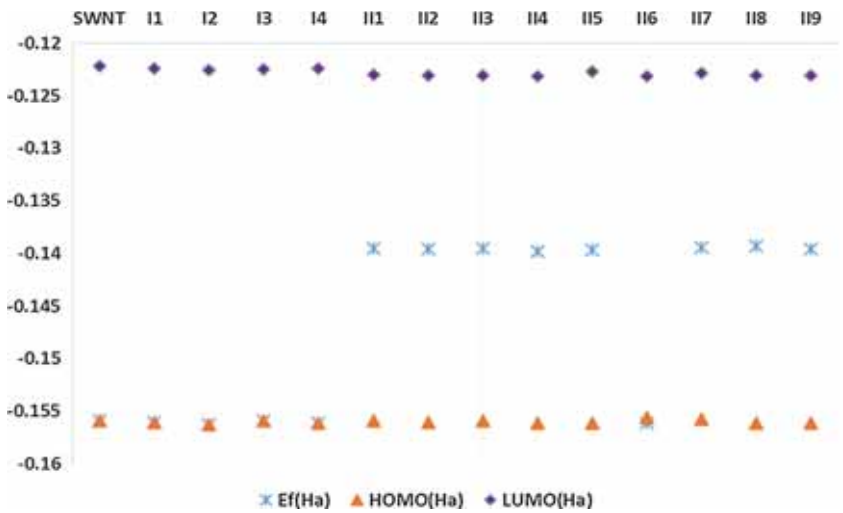

Figure 8. Diagram of the Fermi, HOMO and LUMO energies for SWCNT, I and II models.

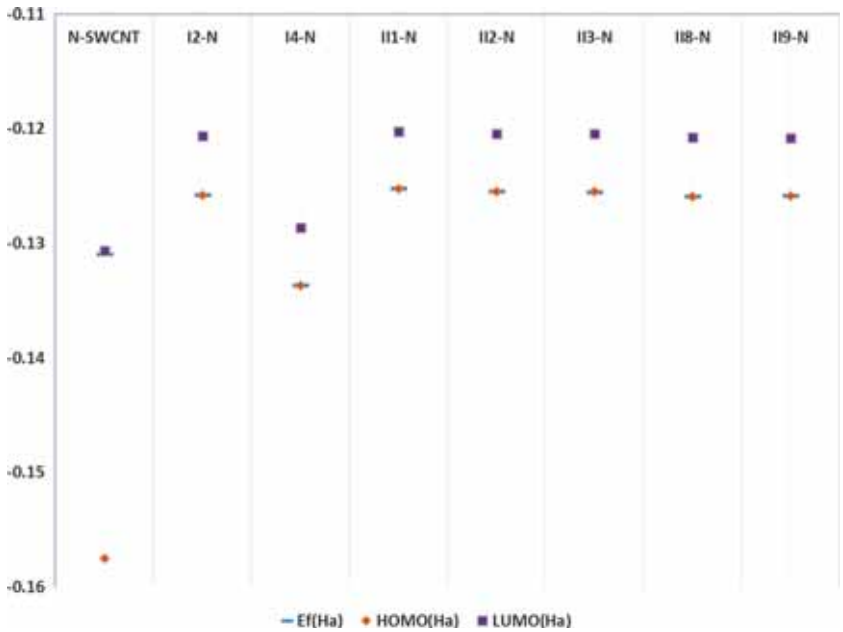

Figure 9. Diagram of the Fermi, HOMO and LUMO energies for N-SWCNT and N-doped models.

The maximal oscillator strength of the pristine models (except II4) are higher than that of SWCNT and doped models (except II9-N) are higher than that of N-SWCNT. The wavelength of transition of H $\rightarrow$ L in SWCNT and pristine models is lower than N-SWCNT and doped models.

The molecular electrostatic potential (MEP) maps are essential for studying and predicting the reactive sites for electrophilic and nucleophilic attacks. The MEP maps were evaluated at the GGA/PW91 level for two directions and are shown in figure 12. The positive regions of the MEP map, shown in blue colour, are associated with nucleophilic reactivity and the negative regions, shown in yellow colour, are associated with electrophilic reactivity. Figure 12 shows that the electrostatic potential (ESP) charges of N_2 molecule(s) in the models of I2, I4, II8 and II9 are negative compared with other models. In Hirshfeld methods, the charges on the N_2 molecule(s) of the models of I2 and I4 in type-I and II8 and II9 models in type-II are more negative than their other models (see table 6). The models of I2, I4, II8 and II9 show adsorption on SWCNT surface. The electrostatic potential charges of N_2 molecule(s) in the I2-N, I4-N, II8-N and II9-N models are negative

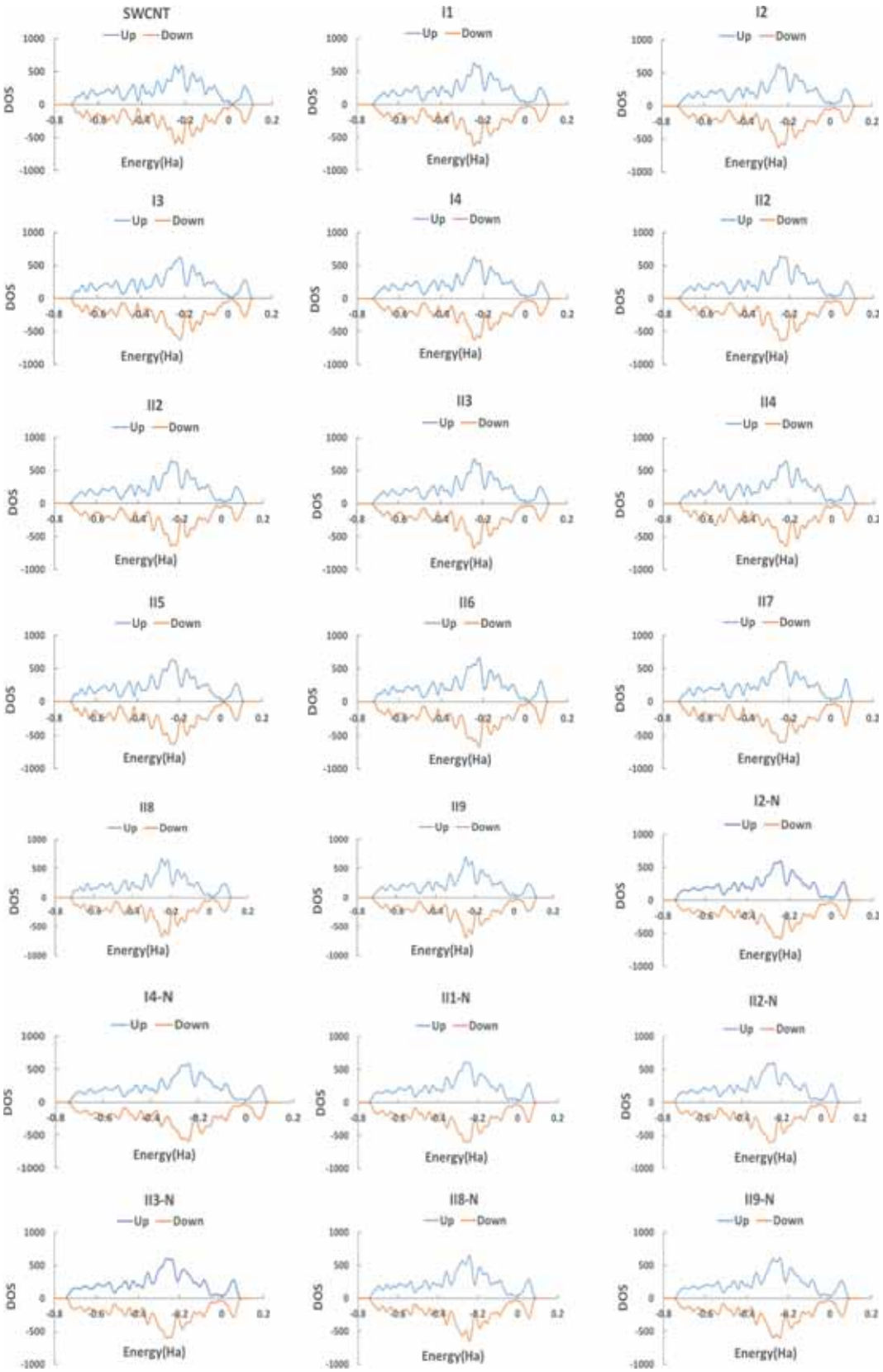

Figure 10. The DOS of spin-up and spin-down electrons of the pristine and N-doped models.

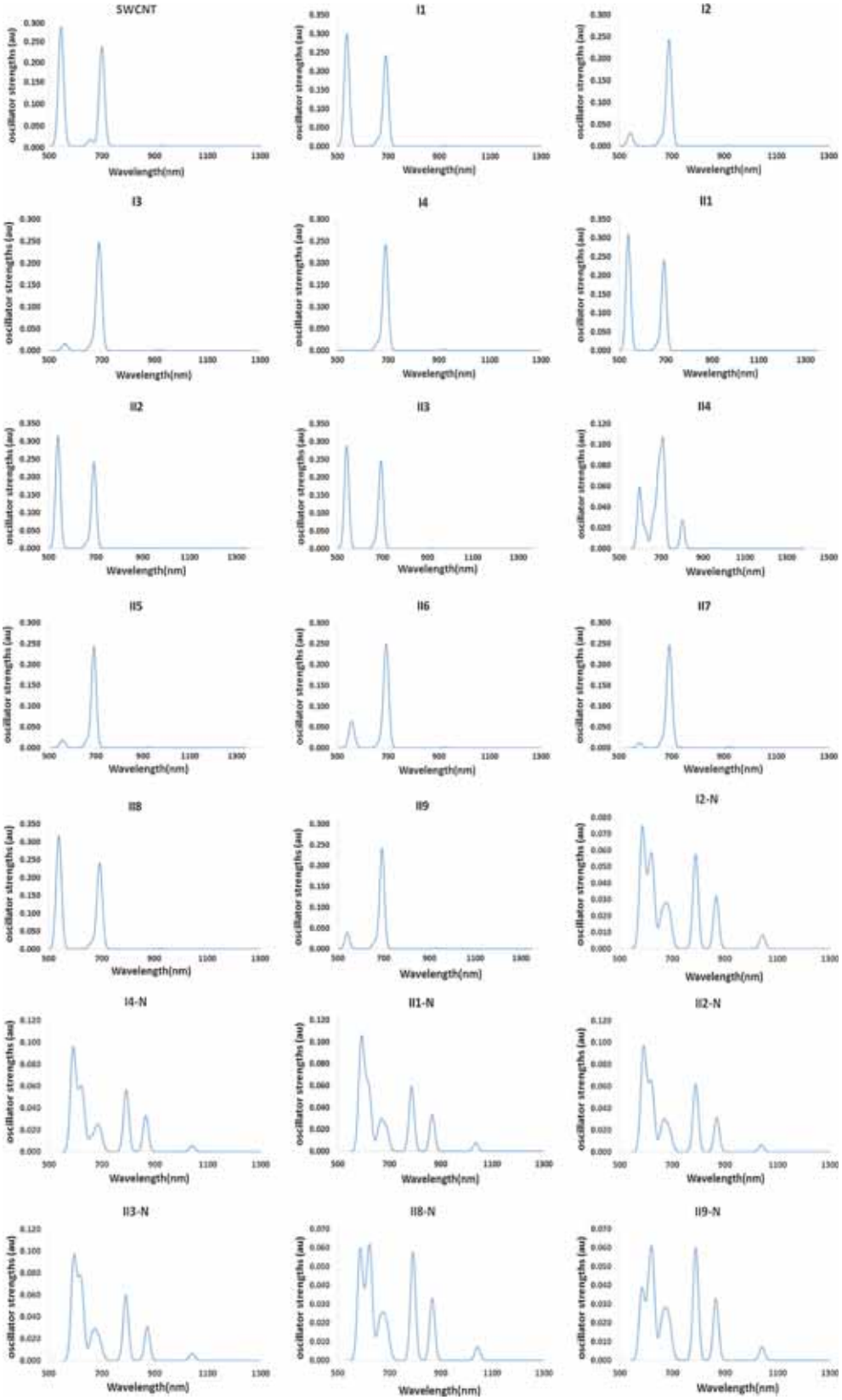

Figure 11. The oscillator strength values in terms of wavelength which were calculated by time-dependent density functional theory (TD-DFT).

Table 9. The oscillator strength and wavelength of electronic transitions of H → L and wavelength of electronic transitions with maximum oscillator strength for pristine models.

Models	Transition	λ (nm)	Oscillator strength	Models	Transition	λ (nm)	Oscillator strength
SWCNT	H → L	1272	0.0000	II3	H → L	1317	0.0000
	H → L + 6	544	0.1490		H − 1 → L	694	0.2444
I1	H → L	1287	0.0000	II4	H → L	1347	0.0001
	H − 1 → L + 1	691	0.2419		H − 1 → L + 1	708	0.0735
I2	H → L	1283	0.0000	II5	H → L	1298	0.0000
	H − 1 → L + 1	690	0.2426		H − 1 → L	692	0.2416
I3	H → L	1293	0.0000	II6	H → L	1333	0.0000
	H − 1 → L + 1	690	0.2454		H − 1 → L	693	0.2453
I4	H → L	1282	0.0000	II7	H → L	1315	0.0000
	H − 1 → L + 1	690	0.2413		H → L + 3	692	0.2422
II1	H → L	1313	0.0000	II8	H → L	1309	0.0000
	H − 1 → L	693	0.2409		H − 1 → L	693	0.2286
II2	H → L	1312	0.0000	II9	H → L	1309	0.0000
	H − 1 → L	693	0.2413		H − 1 → L	693	0.2390

Table 10. The oscillator strength and wavelength of electronic transitions of H → L and wavelength of electronic transitions with maximum oscillator strength for N-doped models.

Models	Transition	λ (nm)	Oscillator strength	Models	Transition	λ (nm)	Oscillator strength
SWCNT-N	H → L	1758	0.0300	II2-N	H → L	1895	0.0011
	H − 1 → L + 2	632	0.0554		H → L + 6	590	0.0909
I2-N	H → L	1905	0.0012	II3-N	H → L	1905	0.0011
	H → L + 6	586	0.0723		H − 1 → L + 2	594	0.0894
I4-N	H → L	1865	0.0013	II8-N	H → L	1909	0.0012
	H − 1 → L + 6	591	0.0907		H → L + 6	586	0.0580
II1-N	H → L	1884	0.0011	II9-N	H → L	1900	0.0012
	H − 1 → L + 2	591	0.0937		H → L + 5	624	0.0519

compared with other models in figure 12. These analyses indicated that charge transfer from N-SWCNT and N-doped models to N_2 molecule(s) is less than charge transfer from SWCNT and pristine models to N_2 molecule(s).

4. Conclusion

The quantum chemical parameters provide information about the chemical reactivity of molecules. The SWCNT type-II6 model has the highest value of electronegativity among the thirteen models that were studied in our work. The adsorption process of the pristine models is exothermic because the adsorption and enthalpy energies of all these models are negative. Also, the Gibbs free energies of the pristine models are negative and the adsorption process is spontaneous. The results reveal that the adsorption energy of the type-II SWCNT models is more negative than that of type-I models. The adsorption of the N_2 molecule on the external wall of a nanotube is found to be more effective than that on its internal wall. The energy gap and global hardness of the SWCNT model of the type-II is lower than that of the type-I model. The energy gap and global hardness of type-II6 model is less than other type-II models. All the models in SWCNT have similar energy gaps and the differences between their energy gaps are very small. Also, there are no changes in the DOS of the conduction and valence bands. We can conclude that the pristine C(5,5) carbon nanotubes cannot be a sensor for identifying N_2 gas. The results of doping of SWCNT and the models of I2 and I4 in type-I and II1, II2, II3, II8 and II9 models in type-II with a nitrogen atom are: (a) energy gap decreases, (b) electric conductivity increases, (c) change of the DOS in the valence band becomes more than the conduction band, (d) the Fermi energies of N-doped models are the same as that of LUMO and Fermi energy of the doped SWNT is equal to its HOMO energy. Therefore, N-SWCNT may be chosen as an appropriate candidate for the adsorption and detection of the N_2 gas molecule(s) when compared with SWCNT.

The SWCNT remains metallic after being doped with a nitrogen atom and the DOSs of the spin-up and spin-down electrons are equal for all values of electron energy which shows that the SWNT, N-SWNT and

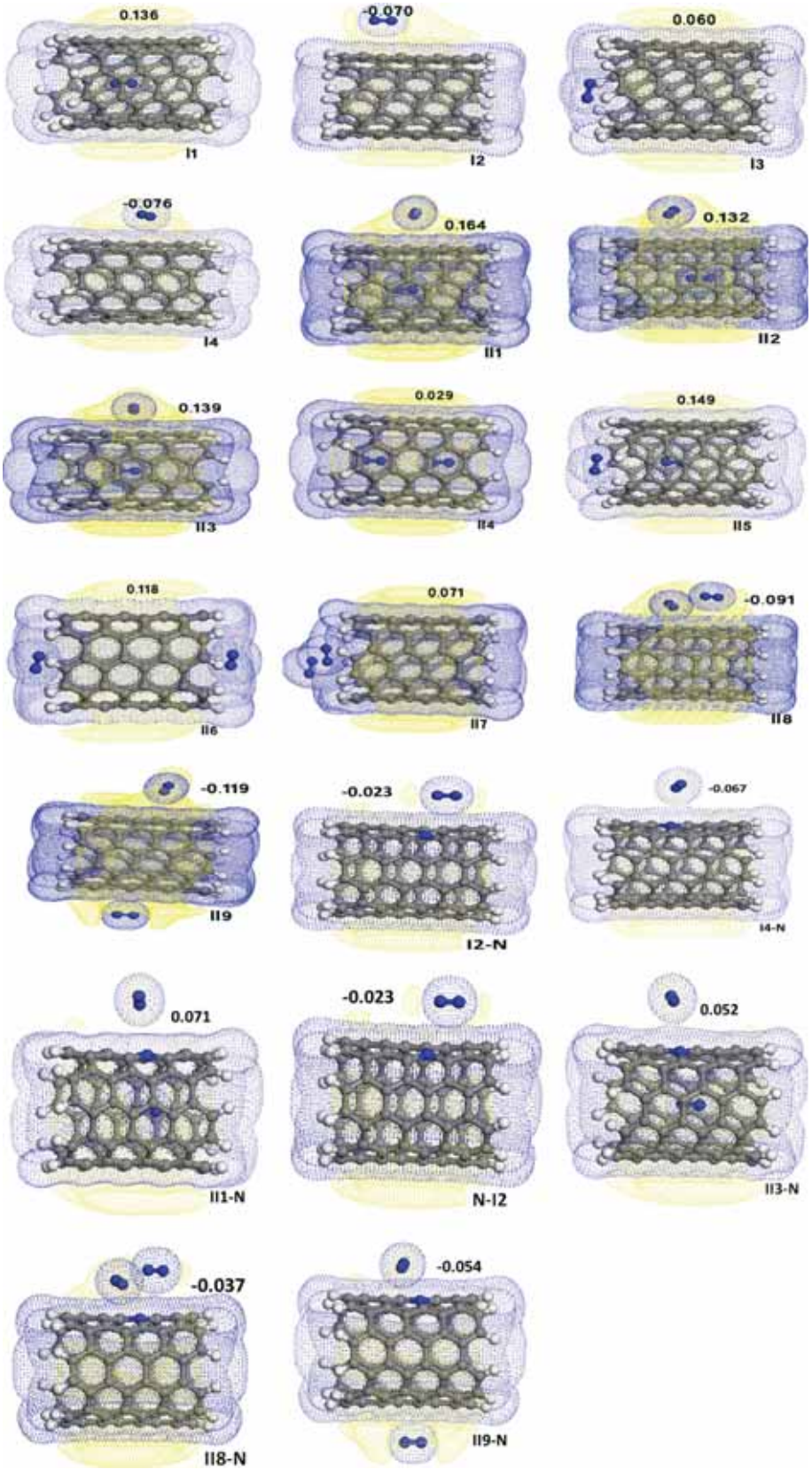

Figure 12. ESP isosurface of compounds studied (isovalue = 0.016, positive values by blue, negative values by yellow colour $DMol_3$/PW91). The numbers are ESP charges for N_2 molecule(s).

all models are antiferromagnetic. The interaction of N_2 molecule(s) with SWCNT and N-SWCNT is physisorption because the interaction has a small adsorption energy, a large adsorption distance and a small charge transfer. The electronic transitions from the HOMO to the LUMO (H → L) have the maximal wavelength and the lowest oscillator strength in each structure. The maximal wavelength of transition of H → L in type-II model is higher than that in type-I model. This wavelength in the models of I2 and I4 in type-I are identical and also II8 and II9 models in type-II. The wavelength of transition of H → L in SWCNT and pristine models is lower than that in N-SWCNT and doped models. In addition, calculations of bond order analysis, atomic charge analysis and electrostatic potential were carried out.

Acknowledgements

This work was supported by 3157 project from the Department of Photonics, Institute of Science, High Technology and Environmental Sciences, Graduate University of Advanced Technology, Kerman, Iran. This article was peer reviewed by Nasser Mirzai Baghini, Imperial College Reactor Centre, Silwood Park, Ascot, Berkshire, United Kingdom.

References

[1] A Hirsch, *Chem. Int. Ed.* **41**(**11**), 1853 (2002)
[2] J L Zang *et al*, *Comput. Mater. Sci.* **46**(**3**), 621 (2009)
[3] J Kong *et al*, *Science* **287**(**5453**), 622 (2000)
[4] S Iijima, *Nature* **354**(**6348**), 56 (1991)
[5] S Ghosh *et al*, *Science* **299**(**5609**), 1042 (2003)
[6] N W Kam *et al*, *J. Am. Chem. Soc.* **127**(**36**), 12492 (2005)
[7] R P Feazell *et al*, *J. Am. Chem. Soc*. **129**(**27**), 8438R (2007)
[8] A Bianco *et al*, *Curr. Opin. Chem. Biol*. **9**(**6**), 674A (2005)
[9] H Kong *et al*, *Catal. Lett.* 1**35**, 83 (2010)
[10] K Kostarelos, *Adv. Colloid Interface. Sci*. **106**(**1**), 147 (2003)
[11] X Zhang *et al*, *J. Phys. Chem. B* **107**(**21**), 4942 (2003)
[12] S C Sorescu *et al*, *J. Phys. Chem. B* **105**(**45**), 11227 (2001)
[13] A A Rafati *et al*, *J. Phys. Chem. C* **112**(**10**), 3597 (2008)
[14] D H Yoo *et al*, *J. Phys. Chem. B* **106**(**13**), 3371 (2002)
[15] E C Et, *Appl. Phys. Lett.* **79**(**23**), 3863 (2001)
[16] Y F Yin *et al*, *Langmuir* **15**(**25**), 8714 (1999)
[17] A Du *et al*, *Nanotechnology* **20**(**37**), 375701 (2009)
[18] Q H Yang, *Chem. Phys. Lett.* **345**(**1**), 18 (2001)
[19] J Zhu et al, *Nanotechnology* **18**(**9**), 095707 (2007)
[20] D H Yoo *et al*, *J. Phys. Chem. B* **107**(**7**), 1540 (2003)
[21] C Kramberger *et al*, *Carbon* **55**, 196 (2013)
[22] G P Lithoxoos *et al*, *J. Supercrit. Fluids* **55**(**2**), 510 (2010).
[23] M Ganji, *Nanotechnology* **19**(**2**), 025709 (2007)
[24] J Zhao *et al*, *Nanotechnology* **13**(**2**), 195 (2002)
[25] B Delley, *J. Chem. Phys*. **92**(**1**), 508 (1990)
[26] J P Perdew and Y Wang, *Phys. Rev. B* **45**(**23**), 13244 (1992)
[27] B Delley, *J. Chem. Phys*. **113**(**18**), 7756 (2000)
[28] X Lu *et al*, *J. Am. Chem. Soc.* **125**(**34**), 10459 (2003)
[29] Y Inada and H Orita, *J. Comput. Chem.* **29**(**2**), 225 (2008)
[30] J Frank, *Introduction to computational chemistry* 2nd edn (Wiley, New York, 2007)
[31] A Musa *et al*, *J. Mol. Struct.* **969**(**1**), 233 (2010)
[32] P K Chattaraj *et al*, *Chem. Rev.* **2**(**111**), PR43 (2011)